*Desalination and Water Treatment*
www.deswater.com

doi:10.5004/dwt.2019.23902

153 (2019) 300–311
June

# The application of modified hematite for removal of carmine red dye: performance and mechanism

Yaqing Zhang, Haibo Liu, Dong Chen, Tianhu Chen*

*Laboratory for Nano-minerals and Environmental Materials, School of Resources and Environmental Engineering, Hefei University of Technology, Hefei 230009, China, email: 1160097448@qq.com (Y. Zhang), liuhaibosky116@hfut.edu.cn (H. Liu), cdxman@hfut.edu.cn (D. Chen), Tel. +86 13956099615, +86 0551 2903990, email: chentianhu@hfut.edu.cn (T. Chen)*

Received 30 July 2018; Accepted 1 February 2019

**ABSTRACT**

Zero-valent iron (ZVI) was prepared by the hydrogen reduction of hematite and characterized by using techniques, such as XRD, XPS, and SEM. Using carmine as a representative dye, the factors, including pH, solid-liquid ratio, reaction time, and temperature, affecting the purification of dye wastewater by the ZVI were investigated. The removal mechanism was discussed based on the experimental data and characterization results. The results showed that under the conditions of pH 2.0 and a solid-liquid ratio of 1 g/L, the decolorizing efficiency by the ZVI reached 99% at a reaction time of 1 h due to the reduction mechanism of ZVI. Another index for the degradation of carmine is TOC, and its maximum removal efficiency is 57% at 24 h mainly due to complexation of $Fe^{2+}$, adsorption of ZVI and precipitation by the corrosion products of iron. The removal of carmine chromaticity by ZVI exhibited first-order reaction kinetics. Meanwhile, the adsorption of isotherms and the kinetics of TOC on ZVI were fit well by the Freundlich and pseudo-second order kinetics, respectively. The results suggested the way for preparing ZVI is feasible and the prepared ZVI is proved to be a promising material for dealing with dyeing wastewater, which benefits the comprehensive application of natural mineral in environmental protection.

*Keywords:* Hematite; Zero-valent iron; Carmine; Dye wastewater; Mechanism

## 1. Introduction

Organic synthetic dyes are widely used in the textile printing and dyeing industry [1,2]. It has been reported that more than 100,000 different commercial dyes are produced per year throughout the world, with a rough estimate of $1\times10^5$–$1\times10^6$ tons produced in total [3]. In China, as it will take a long time for the dye and printing industry to fully achieve the clean production, the control of pollution requires the clean-up of printing and dyeing wastewater. Dye wastewater is one of the most difficult industrial wastewaters to treat because of its high concentration, deep chromaticity, a large amount of refractory organic pollutants, complex composition and large change in water quality. Organic synthetic dyes are the main pollutants in printing and dyeing wastewater. Organic synthetic dyes have several characteristics which pose significant threats to human life and health, including high chromaticity, long residence time, and a lack of biodegradability.

Azo dyes are the most common type of synthetic dyes [4,5] and represent the largest class of dyes used in the textile industry, constituting 60–70% of all dyestuff production [6]. Carmine is a typical azo dye and is one of the most widely used azo synthetic pigments in China. Carmine and Sudan I, which are banned under EU standards, belong to the azo family of pigments, and azo compounds have been reported to be metabolized in vivo to form precursors of mutagenic aromatic amine compounds. The color of the dye depends on its molecular structure, according to the Wiff hair color group theory, and the unsaturated conjugated chain (e.g., –C=C, –N=N–, etc.) of the dye molecules is connected to the opposite group of the electrical properties. After absorbing the energy from light of a certain wavelength, the molecules of the compound polarize and produce a dipole

*Corresponding author.

moment, causing to the transition of valence electrons at different energy levels, to form different colors. Traditional methods for dye removal include biological treatment [7], adsorption [8], coagulation [9], physical treatment [10], flotation [11], electrochemical methods [12,13], nanofiltration [14], biosorption [15], membrane separations [16], and the advanced oxidation methods [17]. At present, the main treatment methods for dye wastewater are the biological methods, physical methods and advanced oxidation methods. Biological methods support environmental protection and sustainable development, but the degradation of dye wastewater is slow due to the long microbial culture cycle, the degradation efficiency is low, which is only applicable in a limited set of environments. The physical method is simple and easy to operate, but it has a high consumption and limited application. The advanced oxidation method is a good method for degradation of dye wastewater, but the energy consumption and dosage consumption are high. In recent years, ZVI has attracted the attention of researchers, because it has good redox and adsorption properties are widely used in various fields. At present, ZVI is mainly used in water treatment, and is considered as one of the most effective materials in the field of water treatment.

Jiasheng Cao et al. [18] used ZVI to degrade azo dyes for the first time, and proposed that ZVI can be applied to in situ restoration of organic dyes in water bodies. Due to the cost-efficiency and easy availability of ZVI and the fact that it causes almost no harm to the human body [19], ZVI has been used for the degradation of organic dyes in recent years [20–23]. Hematite is a natural iron ore with reserves of more than 10 billion t in China. Many reports have indicated that modified hematite could effectively degrade heavy metals [24], organics [25], and ZVI has widespread application in various fields [26,27]. Our experiments on hematite have shown that hematite can yield ZVI after treating with hydrogen reduction at the appropriate temperature. The objective of this paper is to widen the applications of hematite; to investigate the effects of water chemistry such as pH, solid-liquid ratio and temperature on the removal of carmine red dye; and to reveal the mechanism of azo dye removal.

## 2. Experimental

### 2.1. Materials

Natural hematite ($Fe_2O_3$ 69.58 wt%) was collected from Enshi city, Hubei Province, China. The samples were crushed and sieved to the target particle size (<75 μm) and then calcined for 1 h at different temperatures (i.e., 300, 400, 500, and 600°C) under hydrogen conditions. After cooling to ambient temperature, the obtained samples were stored in a drier for further characterization and batch experiments.

Carmine with the molecular formula $C_{20}H_{11}N_2Na_3O_{10}S_3$ (the purity is 99.5%), shown in Fig. 1, was purchased from Tianjin Guangfu Fine Chemical Research Institute of China.

### 2.2. Characterization

FESEM/EDS (field emission scanning electron microscope) measurements were performed on a JEOL JSM-7100F instrument with an energy dispersive X-ray detector. All samples were coated in gold by spraying before analysis.

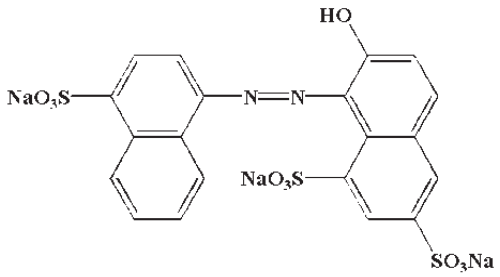


Fig. 1. Molecular structure of carmine in the neutral form.

The XRD patterns of the solid powers were recorded by an X-ray diffractometer (Dangdonghaoyuan 2700 diffractometer) with Cu-Kα radiation. The tube voltage was 40 kV and the current was 40 mA. All XRD patterns were recorded in the range of 5°–70° with a scan speed of 4°/min$^{-1}$ and a divergent slit size of 0.5°. Phase discrimination was carried out by comparison with phase data in the Inorganic Crystal Structure Database (ICSD).

XPS analysis is performed using a Thermo Scientific K-Alpha instrument equipped with an Al-Kα source (10 mA, 14 kV).

IC (ICS-900), with anionic and cationic columns, equipped with dual plunger isocratic pumps, compatible with electrolytic or chemical continuous regeneration microfilm suppressors, Dionex, USA.

HPLC-MS (ACQUITY LCT Premier XE) with sensitivity of SNR (signal-to-noise ratio) > 100:1, the internal standard method of mass accuracy is less than 2 ppm, and the external standard method is less than 5 ppm. The intermediate product was analyzed by liquid chromatography-mass spectrometry and the structure of the intermediate product was analyzed.

### 2.3. Batch experiments

#### 2.3.1. Effect of pH

In a 50 mL centrifuge tube, 50 mg/L carmine solutions were put into 0.01 mol/L NaCl background electrolyte (40 mL). After adjusting the pH of the solution to 1, 2, 3, 4, or 5, 0.04 g of reduced hematite was added. The pH of the solution was adjusted with 0.1 mol/L HCl and NaOH solutions. After the designed reaction time, the absorbance of the supernatant at a wavelength of 508 nm was measured by an ultraviolet-visible spectrophotometer and the TOC concentration of the supernatant was tested by a German Jena Multi type N/C2100 TOC analyzer.

#### 2.3.2. The effect of the solid-liquid ratio

The effect of ZVI dosage was studied under the conditions of 298 K and pH 2 by adding 0.02 g, 0.04 g, 0.08 g, 0.2 g, 0.32 g, 0.4 g, or 0.8 g of reduced hematite solids to the carmine solution, which with an initial concentration of 50 mg/L and a volume of 40 mL, that is, the solid-liquid ratio is 0.5 g/L, 1 g/L, 2 g/L, 5 g/L, 8 g/L, 10 g/Land 20

g/L.Then the absorbance and TOC of the supernatant were measured by centrifugation after 24 h of reaction.

#### 2.3.3. The effect of time

The effect of reaction time on the degradation of carmine by ZVI was studied. Under the conditions of 298 K and pH 2 by adding 0.04 g of reduced hematite solids to the 40 mL of a 50 mg/L carmine solution. Sampling at the following points: 10 min, 30 min, 60 min, 120 min, 240 min, 480 min, 1440 min, and then the samples were processed to test absorbance A and TOC.

#### 2.3.4. Isotherms

Adsorption isotherms were performed at pH 2 and temperatures 298 K, 306 K, or 314 K. In these experiments, a constant mass of reduced hematite (0.04 g) was mixed with 40 mL solution containing carmine concentrations in the range of 5–50 mg/L. Suspensions were shaken until adsorption equilibrium was reached. Then the samples were centrifuged. The residual concentration in the solution was analyzed, and the experimental data were fitted with Langmuir and Freundlich models.

#### 2.3.5. Kinetics

Reduced hematite (0.04 g) was added to in a 50 mg/L carmine solution (40 mL) at pH 2 and mixed by rotation. Samples were collected and centrifuged at 10 min, 20 min, 30 min, 40 min, 60 min, 90 min, 120 min, 240 min, 480 min and 1440 min. Then the concentration of carmine was detected by spectrophotometry, and the TOC concentration determined by a TOC tester. The kinetics data were fitted using a pseudo-first order kinetic model and a pseudo-second order kinetic model.

In the paper, ZVI has two indicators for the degradation of carmine, one of which is chromaticity and the other is TOC. Correspondingly, reaction kinetics and adsorption kinetics were used to study the experimental data.

### 2.4 Analytical methods

Decolorizing activity was expressed in terms of decolorizing efficiency (%) based on measurements taken at the maximum absorption wavelength of carmine, λ = 508 nm. Total organic carbon was expressed in terms of TOC removal efficiency (%). The efficiencies were calculated as follows:

$$\textit{Decolorizing efficiency}\ (\%) = \frac{1 - A}{A_0} \tag{1}$$

$$\textit{TOC removal efficiency}\ (\%) = \frac{1 - TOC}{TOC_0} \tag{2}$$

where A is the ultimate residual absorbance, $A_0$ is the initial absorbance, $TOC_0$ is the initial total organic carbon, and TOC is residual total organic carbon, calculated by TOC difference subtraction to the difference between total carbon and inorganic carbon.

## 3. Results and discussion

### 3.1. Characterization of ZVI

The solid product of ZVI and the product after reaction with carmine were further characterized by centrifugation, freeze drying, and vacuum packaging. Fig. 2A and B show the SEM images of ZVI particles before and after use. Fig. 2A shows porous structures of the prepared ZVI derived from the reduction of hematite at high temperature, which facilitates the adsorption of the organic carbon in dye molecules. Fig. 2B shows the morphology of ZVI after the reaction, revealing that the morphology is mainly sheet-like with an interlayer structure of green rust. According to the EDS display of Fig. 2B, Fe, O, N and Na are the main elements in the solid after the reaction, which indicates that carmine molecules enter the green embroidery layer and precipitate in the layer. Fig. 2C shows XRD patterns of hematite, hematite after calcination at different temperatures for 1 h and the reacted ZVI. The reflections of hematite and quartz are found in the raw ore. At calcination temperatures below 300°C, the hematite basically maintains its original structure. When the calcination temperature reaches 400°C, almost all of hematite transforms into magnetite. With a further increase in the calcination temperature to 500°C, the reflections of magnetite clearly decrease and a new substance identified as ZVI can be observed. When the calcination temperature reaches 600°C, the reflections of ZVI become stronger, while magnetite almost disappears. The Scherrer formula was used to determine the particle size of reduced hematite at 600°C to be 33.73 nm. As seen in Fig. 2C, with increasing temperature, the reflections of ZVI gradually become sharp. From the point of view of energy, 600°C was selected as the optimal calcination temperature for ZVI for degradation of carmine dye wastewater. X-ray photoelectron spectroscopy (XPS) is well-known as an effective tool for analyzing the interactions between adsorbates and adsorbents [28]. XPS-based spectral lines can be used for qualitative elemental analysis, and all elements except H and He can be identified according to the positions of the characteristic spectral lines appearing in the energy spectrum. Fig. 2D shows the analysis of elemental valence of the ZVI before and after reaction. According to XPS spectra, the characteristic binding energies of $Fe^0$, $Fe^{2+}$ and $Fe^{3+}$ were observed to be 706.7 eV, 710.6 eV and 711.38 eV [29], respectively, in the sample before reaction. However, after the reaction, ZVI and divalent iron were gradually oxidized to trivalent iron, and iron hydroxide was formed [30].

### 3.2 Effect of pH

The pH value of the solution is an important parameter affecting the reaction efficiency of ZVI degradation of organic dye [31]. Therefore, controlling the pH value of the dye wastewater is of great significance for degradation of the dye in wastewater, as the pH value of real dye wastewaters fluctuates significantly. Research results have shown a high degree of correlation between the reaction rate of ZVI degradation of organic dyes and the pH value of the solution [32], with previous studies showing that the dye wastewater degrades better under acidic conditions. As shown in Fig. 3, the effect of solution pH on the chroma and TOC degradation by the ZVI was displayed and the variation of solution was also exhibited.

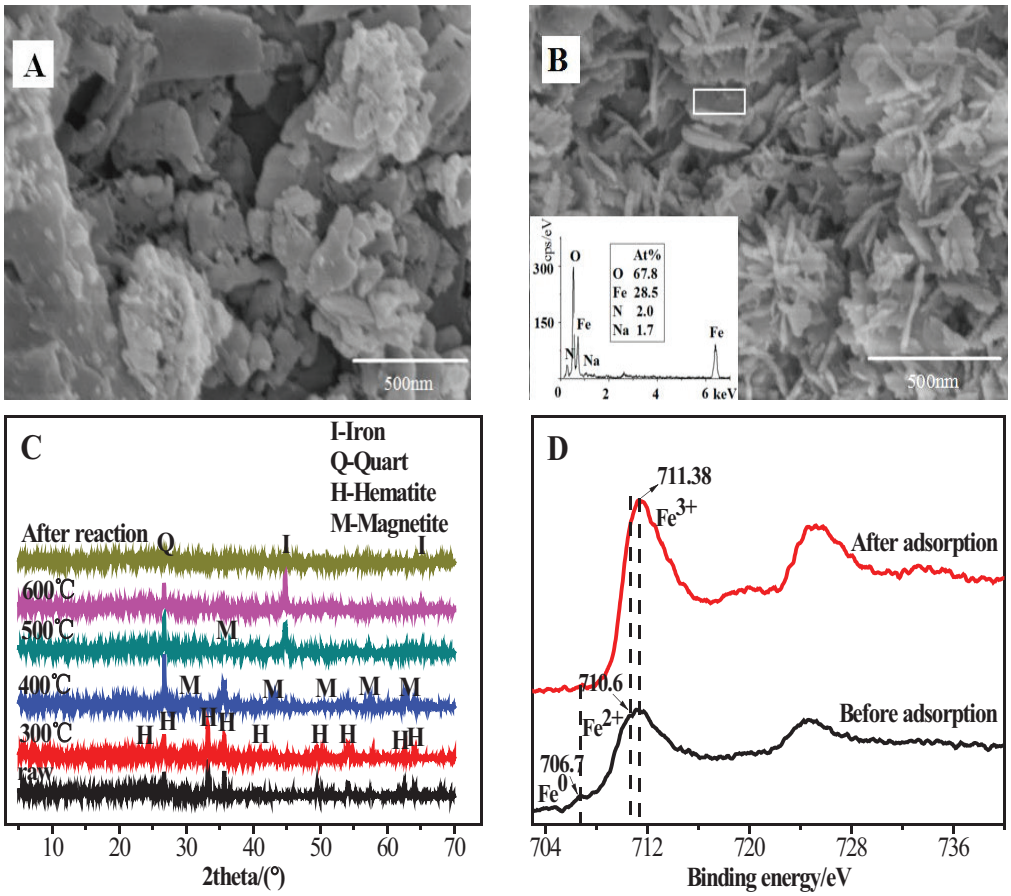


Fig. 2. Characterization of ZVI before and after use. (SEM images of ZVI before (A) and after (B) adsorption; (C) XRD patterns; (D) XPS).

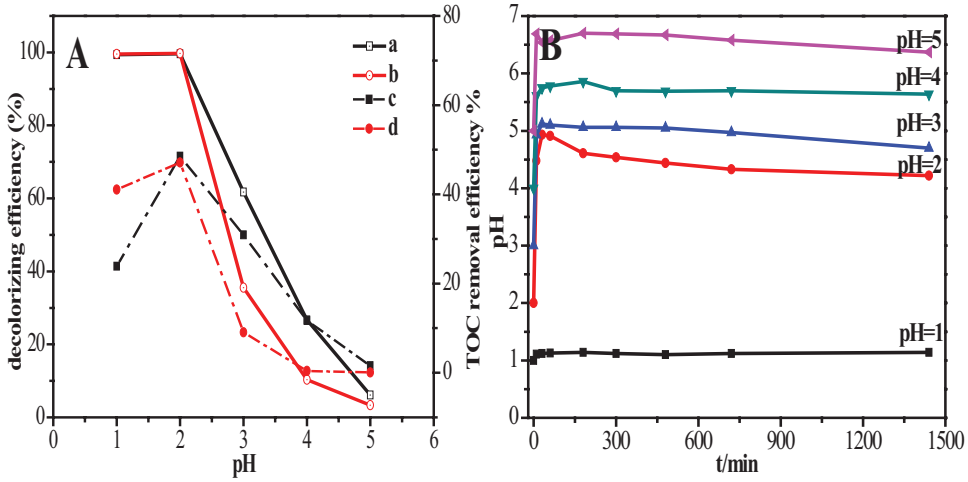


Fig. 3. The effect of pH and variations of pH over residence time.

A: The treatment effect of pH value on chromaticity and TOC; B: Variation of initial pH during reaction. a: 20 mg/L chromaticity removal efficiency; b: 50 mg/L chromaticity removal efficiency; c: 20 mg/L TOC removal efficiency; d: 50 mg/L TOC removal efficiency

In Fig. 3A, the decolorizing efficiency of ZVI on the carmine dye wastewater is greater than 99% when the pH value is less than 2. In detail, the decolorizing rates of the carmine solutions at concentrations of 20 mg/L and 50 mg/L,when the pH value was 1, the decolorizing effects were 99.39% and 99.58%,

respectively, while the decolorizing effects of the carmine solution with pH 2 were 99.59% and 99.75%, respectively. However, the decolorizing effect becomes significantly worse when the pH value is greater than 2. Under strong acidic conditions, the ZVI and carmine dye molecules are more likely to undergo an oxidation-reduction reaction, destroying the color-assisting group of the dye, promoting azo bond breakage, and forming amine-based organic substances. Amine-based organic matter is easily decomposed, which dilutes the chromaticity in the wastewater. It is easy to form precipitate (Ksp[$Fe(OH)_3$] = $3.0\times10^{-38}$) deposits on the surface of ZVI that hinder the progress of the reaction under weak acidic conditions and then reduce the activity of ZVI [33].

As shown in Fig. 3A, the TOC removal is best when the pH is 2. When the pH value is 1, the lower TOC removal efficiency may be due to the excessive acidity passivating the surface of the iron and forming a protective film, thereby preventing the reaction from proceeding and resulting in a lower removal effect. However, when pH value increased to 3–5, the TOC removal effect decreased gradually because the weaker acidity decreased the rate of reaction between iron and carmine dye. Overall, pH 2 is the optimal pH to ensure both high decolorizing effect and good TOC removal efficiency.

Fig. 3B shows variations in pH over residence time for different initial pH conditions. At pH 1, the pH of the solution at 24 h was almost unchanged. The acidity of the solution is so strong that the extra $H^+$ does not participate in the reaction, and the pH value of the solution does not change significantly. For initial pH values of 2–5, the pH value of the solution suddenly increases to reach the equilibrium value and then decreases slightly. This result occurs because the consumption of large amounts of $H^+$ in the initial reaction stage makes the solution pH value rise abruptly. This increase in pH can be attributed to the corrosion of ZVI, increasing the hydroxyl ion concentration and producing iron hydroxide precipitation [34]. Then, the reaction gradually reaches stability as the time increases. A large amount of $H^+$ is no longer needed, and the pH value of the solution exhibits little additional change.

### 3.3. The effect of the solid-liquid ratio

Fig. 4 shows the effect of the solid-liquid ratio on the degradation of carmine. The decolorizing efficiency increases rapidly when the solid-liquid ratio is less than 1 g/L. While the solid-liquid ratio exceeds 1 g/L, the chromaticity removal efficiency was basically stable at 99%. Meanwhile, the TOC removal efficiency rapidly increased at a solid-liquid ratio of 0.5–1 g/L, slowly increased at a solid-liquid ratio of 1–8 g/L, and the removal efficiency gradually stabilized at 57% when the solid-liquid ratio was greater than 8 g/L. Previous studies have shown that excessive ZVI can inhibit the degradation of dyestuffs, and that excess ZVI will cause the iron ion to reunite or accumulate, thus reducing the specific surface area [7].

### 3.4. The effect of time

To further investigate the dynamic process of degradation of carmine by ZVI, the reaction kinetic equation is used to analyze the data. The kinetic parameters are shown in Fig. 5. Fig. 5A shows the chromaticity removal capacity

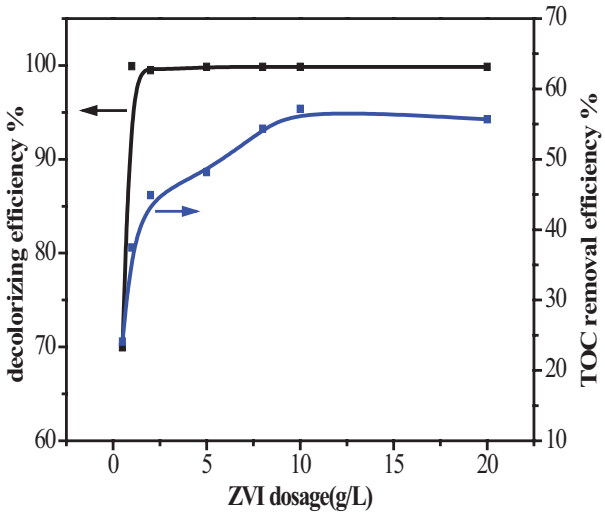


Fig. 4. Effect of ZVI dosage on degradation of carmine dye wastewater.

over time. The decolorizing efficiency gradually increased within 60 min, reaching more than 99%, indicating that at the initial stage of the reaction, ZVI gradually degraded the carmine dye molecules to destroy the azo double bonds in the dye molecules, and reached the best removal effect value in 60 min. The decolorizing efficiency, however, begins to decrease after 60 min because the $Fe^{2+}$ and $Fe^{3+}$ generated by the reaction participate in the reaction, and $Fe(OH)_2$ and $Fe(OH)_3$ precipitates are inefficient, resulting in the solution becomes turbid and the decolorizing efficiency is reduced. After 60 min, the supernatant was centrifuged and 0.1 mol/L NaOH was added to the supernatant to adjust the pH of the system to approximately 10 to make the $Fe^{2+}$ in the system sufficiently reactive, generating $Fe(OH)_3$ precipitation. This solution was then allowed to stand for 240 min and the supernatant was tested, displaying that the color removal effect reached more than 99%. The results showed that the chromaticity was affected by the formation of $Fe^{3+}$. Fig. 5B shows the removal of TOC from carmine solution by ZVI. As the reaction proceeds, the TOC removal efficiency gradually increases. In the first 120 min, TOC removal efficiency increased gradually, and after 120 min the TOC removal efficiency remained between 55%–70%. This is because the reduction of carmine dye molecules by ZVI causes carmine dye molecules to breakdown into small molecular substances by breaking azo bonds, but it is difficult to degrade these small molecular substances furtherly.

### 3.5. Adsorption isotherms

It is known that a chemical reaction is generally sensitive to the changes in temperature [35]. Fig. 6 shows the effect of temperature on chromaticity. The decolorizing efficiency increases with the increase of temperature, and can reach more than 99% after 1440 min, showing that the complete degradation of carmine dye wastewater by the ZVI can be realized under room temperature. The increase in temperature increases the activity of ZVI, accelerates the reaction rate, and hence increases the decolorizing

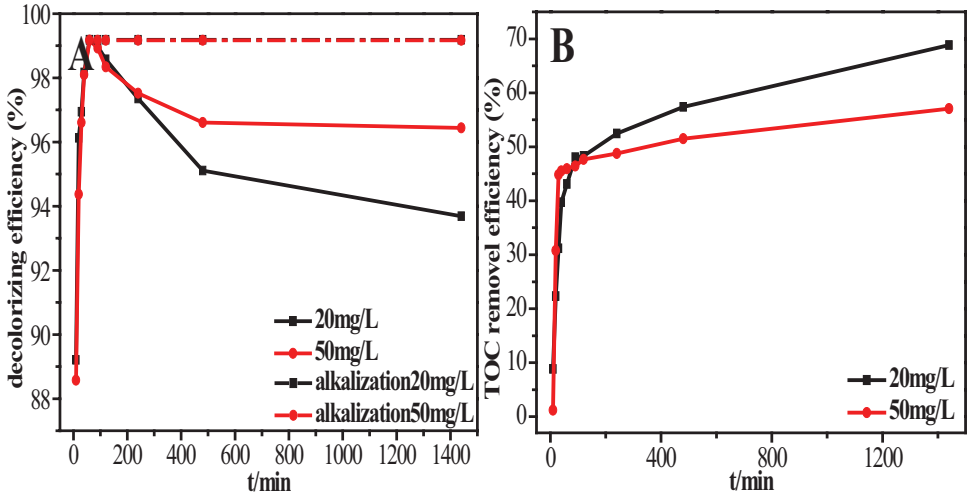


Fig. 5. Degradation of carmine by ZVI over time. A: decolorizing efficiency. B: TOC removal efficiency.

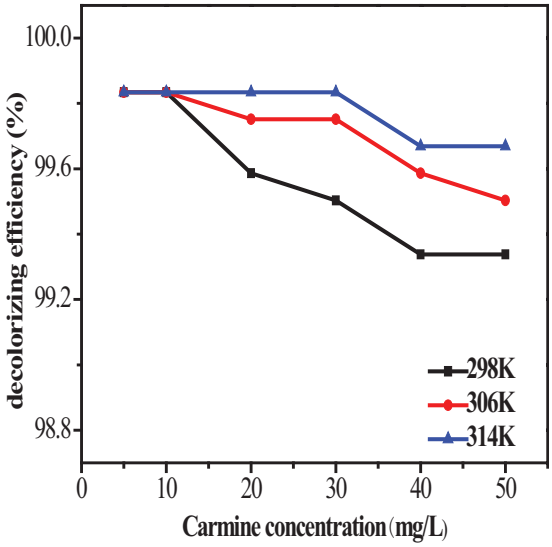


Fig. 6. Effect of temperature on degradation of carmine dye wastewater.

efficiency. Therefore, the decolorizing efficiency at 314K is greater than that of 298K. Moreover, the degradation efficiency experiences a slight decrease with increasing initial concentration of dye, which should be affected by the limited ZVI amount.

The same mass of reduced hematite was added to carmine solutions with different initial concentrations (5–50 mg/L) at pH 2 and temperatures of 298 K, 306 K, and 314 K, and the data were fitted according to the test results. As shown in Fig. 7, the TOC adsorption isotherm of carmine dye wastewater on ZVI was obtained, and the experimental data were fitted linearly with Freundlich and Langmuir isotherms, with the results shown in Table 1.

The linear forms of the Langmuir and Freundlich models were given in Eq. (3) [36] and Eq. (4) [37], respectively:

$$Q_e = \frac{Q_m K_L C_e}{(1 + K_L C_e)} \quad (3)$$

$$Q_e = K_F C_e^{1/n} \quad (4)$$

where $C_e$ (mg·L$^{-1}$) is the residual dye concentration, $Q_e$ (mg·g$^{-1}$) is the residual dye concentration, $Q_m$ (mg·g$^{-1}$) is the maximum adsorption capacity of adsorbent at complete monolayer coverage, $K_L$ (L·mg$^{-1}$) is a Langmuir constant, 1/n is the heterogeneity of the adsorption sites, and $K_F$ represents the equilibrium coefficient describing the partitioning of the absorbent between the solid and liquid phases over the concentration range studied. As observed in Fig. 7A and B, the adsorption of TOC on ZVI was fitted very well by the Freundlich model.

Table 1 shows the fitting parameters of the Langmuir and Freundlich equations for the experimental results. Base on the fitting coefficient $R^2$, the Freundlich equation describes the TOC adsorption process of carmine solution on ZVI more accurately, and shows that this adsorption process is more prone to multi-layer heterogeneous adsorption. The constant $K_F$ increases significantly from 1.886 to 1.963 mg·g$^{-1}$ as the temperature rises from 298 to 314 K relates to the adsorption capacity. This illustrates that the adsorption of carmine by ZVI is an endothermic [38]. The Langmuir model is widely used in many fields, and is suitable for single-layer adsorption and limited surface adsorption sites. In the Freundlich model, it is generally accepted that adsorption is relatively easy when 1/n is between 0.1 and 1.0, whereas adsorption is difficult when 1/n is greater than 2, and 1/n is less than 1 in this experiment [39].

### 3.6. Reaction kinetics

The redox reaction mechanism of the ZVI degradation of carmine color was further explored by analyzing the reaction kinetics. The experimental data were fitted with zero-order, first-order and second-order reaction kinetics, and the results were as follows:

Equation of zero-order reaction:

$$C_e = C_0 - k_0 t \quad (5)$$

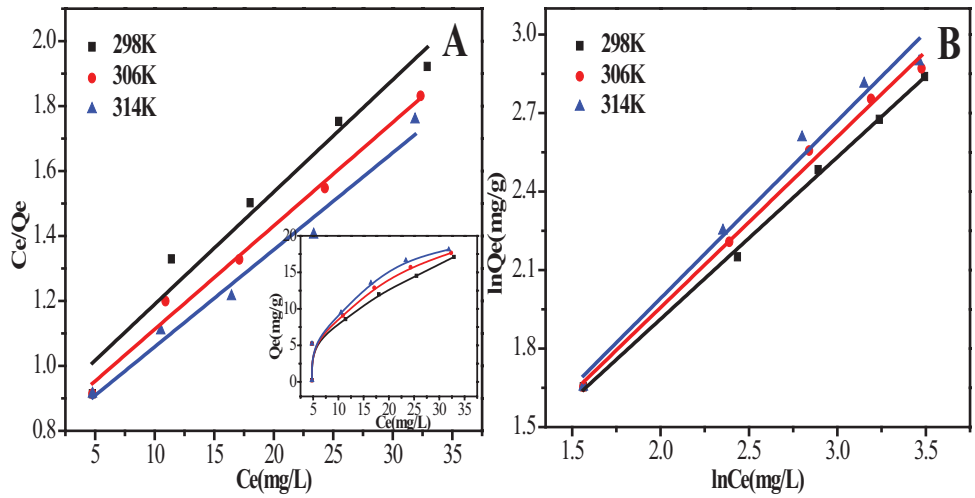


Fig. 7. A: Langmuir fitting curve; B: Freundlich fitting curve.

Table 1
Langmuir and Freundlich model of TOC adsorption

| Temperature (K) | Langmuir | | | Freundlich | | |
|---|---|---|---|---|---|---|
| | $Q_m$ (mg·g$^{-1}$) | $K_L$ (L·mg$^{1}$) | $R^2$ | $K_F$ (mg·g$^{-1}$) | 1/n | $R^2$ |
| 298 | 28.93 | 0.041 | 0.950 | 1.963 | 0.619 | 0.998 |
| 306 | 31.38 | 0.040 | 0.986 | 1.918 | 0.653 | 0.992 |
| 314 | *33.46* | 0.039 | 0.975 | 1.886 | 0.679 | 0.980 |

Table 2
Reaction kinetics - related parameters

| | Zero-order reactions | | First-order reaction | | Second-order reaction | |
|---|---|---|---|---|---|---|
| $C_0$ (mg·L$^{-1}$) | $R^2$ | $K_0$ (mg·L$^{-1}$·min$^{-1}$) | $R^2$ | $K_1$ (min$^{-1}$) | $R^2$ | $K_2$ (L·mg$^{-1}$·min$^{-1}$) |
| 20 | 0.8553 | –0.0339 | 0.9572 | –0.0659 | 0.9586 | 0.0693 |
| 50 | 0.8562 | –0.1537 | 0.9960 | –0.0662 | 0.9946 | 0.0683 |

where $C_0$ is the initial dye concentration (mg·L$^{-1}$), $C_e$ is the residual dye concentration (mg·L$^{-1}$), $k_0$ represents the observed pseudo zero-order rate constant (mg·L$^{-1}$·min$^{-1}$) and $t$ is the residence time (min). The rate of that zero-order reaction is independent of the concentration of the reactants and is influenced by other factors such as the solubility of the reactants or the degree of illumination for some photochemical reactions.

First-order kinetic reaction equation [40]:

$$\ln\frac{C_e}{C_0} = -k_1 t \tag{6}$$

where $k_1$ (min$^{-1}$) is the observed first-order rate constant and $C_0$ is the initial dye concentration (mg·L$^{-1}$). Therefore, $k_1$ can be calculated from the regression of ln ($C_e/C_0$) versus residence $t$.

Second-order kinetic reaction equation [36]:

$$\frac{-dC_e}{dt} = k_2 C_e^{\,2} \tag{7}$$

where $k_2$ is the second-order reaction rate constant (L·mg$^{-1}$ min$^{-1}$), and the reaction rate is proportional to the square of the reaction concentration. The curve of the linear relationship can be drawn from the slope of ln ($1/C_e$–$1/C_0$) and $t$(min). The amended second-order model equation can be expressed:

$$\ln\left(\frac{1}{C_e} - \frac{1}{C_0}\right) = k_2 t \tag{8}$$

The fitted parameters of reaction kinetic models are listed in Table 2. The correlation coefficients $R^2$ is ranging from 0.8553 to 0.8562 for the zero-order model, from 0.9572 to 0.9960 for the first-order model and from 0.9586 to 0.9946 for second-order model. This indicates that the chromaticity of ZVI-degraded carmine dyes conforms to the first-order and second-order kinetic models. Previous studies have shown that the degradation of dyes by ZVI belongs to the reduction process and can be well described by the pseudo-first-order kinetic model. However, the kinetics could

be fitted with not only the first-order model but also the second-order model in this work [41]. These results indicate that degradation involves adsorption and simultaneous redox processes.

### 3.7. Adsorption kinetics

Fig. 8 shows the adsorption process of TOC in carmine solution with ZVI concentrations of 20 mg/L and 50 mg/L at a temperature of 298 K. The solid-liquid ratio is 1 g/L and the pH value is 2. With increasing time, the adsorption capacity gradually increased. Different kinetic models correspond to different reaction mechanisms, and two kinetic adsorption models are often used to analyze such data. To study the adsorption effect of ZVI on carmine solution, the experimental data were fitted with the pseudo-first-order Eq. (9) and the pseudo-second-order Eq. (10).

$$\ln(Q_e - Q_t) = \ln Q_e - \frac{k_1 t}{2.303} \tag{9}$$

$$\frac{t}{Q_t} = \frac{1}{k_2 Q_e^2 + \frac{t}{Q_e}} \tag{10}$$

where $Q_e$ (mg·g$^{-1}$) and $Q_t$ (mg·g$^{-1}$) are the adsorption equilibrium and adsorption capacity of ZVI to total organic carbon at time t, respectively. $k_1$ (min$^{-1}$) and $k_2$ (g·mg$^{-1}$·min$^{-1}$) are the pseudo-first-order and pseudo-second-order kinetic rate constants.

As seen from Table 3, the correlation coefficient of the pseudo-second-order kinetic equation is better than that of pseudo-first-order adsorption. The pseudo-second-order kinetic equation better describes the adsorption process of carmine on ZVI, and the correlation coefficient is greater than 0.99. The results of pseudo-second-order kinetics found in the study are consistent with the findings of some earlier works [42,43]. With increasing concentration of carmine, the equilibrium rate constant $k_2$ also increases gradually, indicating that chemisorption is the main step in limiting the rate of reaction during most of the adsorption of ZVI, which due to covalent forces or electron exchange between the adsorbent and carmine [44]. The pseudo-second-order kinetic model includes all adsorption processes, such as external liquid membrane diffusion, surface adsorption and particle internal diffusion.

### 3.8. Removal mechanism

*HPLC-MS* analyses were carried out to investigate intermediate products formed during the degradation process at different reaction times. Fig. 9A shows the mass spectrum of dye samples collected at 0 min, with a major peak at 583 m/z. Fig. 9B is a mass spectrum of degraded carmine after 240 min, in which the peak at 583 m/z disappears replaced by two new peaks of 468 m/z and 478 m/z, and two peaks appear at 911 m/z and 1344 m/z representing a polymer made up of small molecule degradation products. Fig. 9C is a mass spectrum of carmine degradation after 480 min, indicating no change in the position of the peaks compared with 240 min, but with the relative intensities of the 468 m/z and 478 m/z peaks reversed. This figure shows that the mass-to-charge ratio of 468 m/z increases and the mass-to-

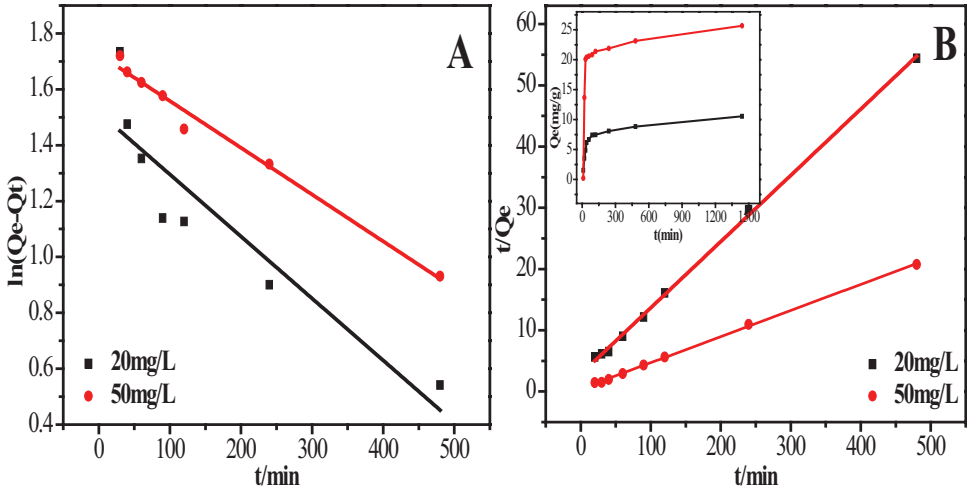


Fig. 8. A: pseudo-first order dynamics; b: pseudo-second-order dynamics.

Table 3
Kinetic parameters of degradation of carmine dye wastewater by ZVI

| Initial concentration (mg·L$^{-1}$) | Pseudo-first-order | | | Pseudo-second-order | | |
|---|---|---|---|---|---|---|
| | $Q_e$ (mg·g$^{-1}$) | $k_1$ (min$^{-1}$) | $R^2$ | $Q_e$ (mg·g$^{-1}$) | $k_2$ (g·mg$^{-1}$·min$^{-1}$) | $R^2$ |
| 20 | 4.559 | 0.005 | 0.809 | 9.383 | 0.0034 | 0.996 |
| 50 | 5.616 | 0.004 | 0.982 | 23.44 | 0.0043 | 0.999 |

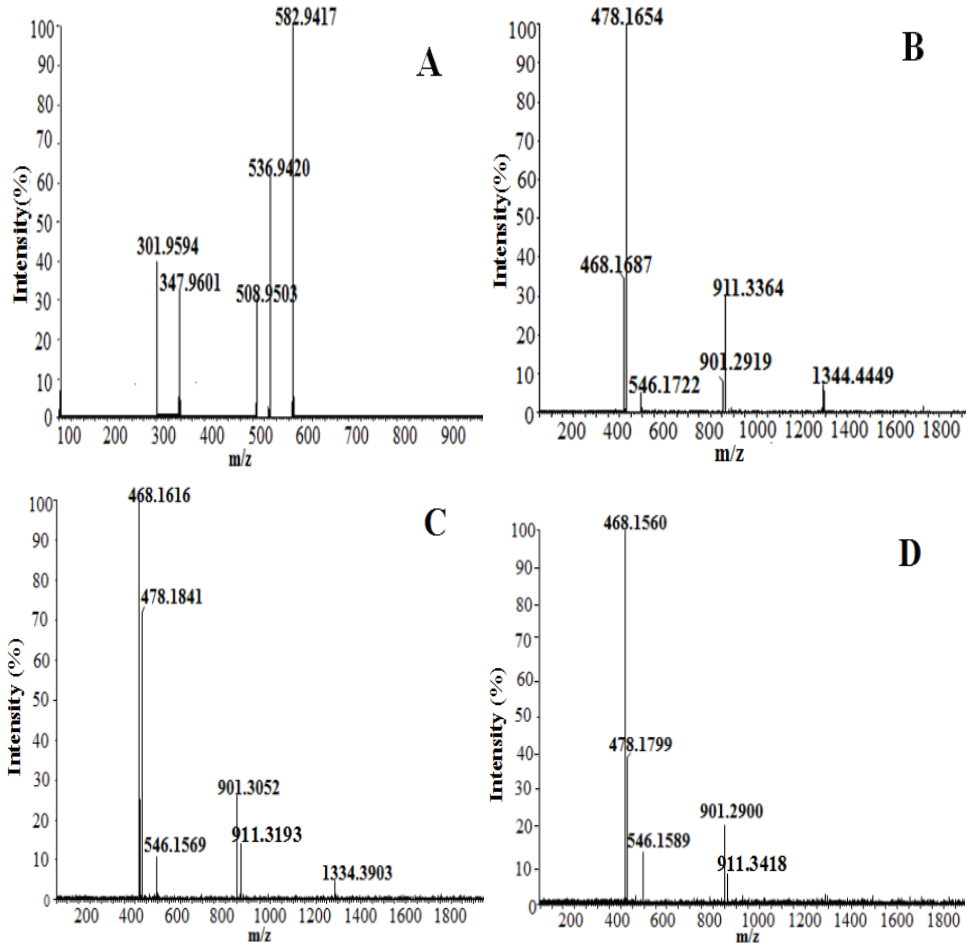


Fig. 9. Mass spectra of degraded carmine by zero-valent iron at different time. A. 0 min; B. 240 min; C. 480 min; D. 1440 min.

charge ratio of 478 m/z decreases as the reaction progresses from 240 min to 480 min. Meanwhile, as time goes on, the mass-to-charge ratio of 911 m/z and 1334 m/z also experiences an obvious decrease, which is in consistence with the variation of 468 m/z and 478 m/z. Fig. 9D is a mass spectrum of carmine degradation after 1440 min, exhibiting little change in the reaction product compared with that at 8 h. In detail, the peak value of mass-charge ratio 478 m/z is weaker than that of mass spectrometry with reaction time of 480 min, which indicates that the intermediate product is unstable. The polymer with a mass to charge ratio of 1334 m/z disappeared. The results showed that the carmine molecules were degraded into small molecules during the reaction, which was consistent with the conclusion that ZVI degraded the chromaticity.

To design a set of test in the experiments, the reduced hematite in the pure water released $Fe^{2+}$ was measured to be 172.9 mg/L. Then, $FeSO_4$, with a mass concentration of 172.9 mg/L of $Fe^{2+}$, was used to degrade carmine for 1440 min instead of reduced hematite, and the results showed that the degradation effect of chromaticity and TOC was about 10%. This indicates that $Fe^{2+}$complexed with carmine, about 10% of the whole TOC removal.

In order to further explore the role of ZVI in experiment, three groups of experiments were designed. Table 4 shows

Table 4
Sulfonate concentration and sulfate concentration by ion chromatography

| Group | Sample | Sulfonate ion concentration (mg/L) | Sulfate ion concentration (mg/L) |
|---|---|---|---|
| 1 | $Fe^0$, $H_2O$, pH = 2 | 0 | 0 |
| 2 | Carmine, pH = 2 | 0 | 0 |
| 3 | $Fe^0$, carmine pH = 2 | 0.0620 | 0.865 |

three groups of samples that were pretreated to remove metal ions under different experimental conditions. Groups 1 and 2 were blank controls. In group 1, only ZVI (0.04 g) was reacted with deionized water (40 mL) at pH 2 for 1440 min. In the second group, only carmine solution (50 mg/L) was used in the experiment at pH 2. In the third group, both ZVI (0.04 g) and carmine solution (50 mg/L) was used in the experiment. The concentrations of the sulfonate and sulfate ions in three groups of samples were measured by an ICS-900 type ion chromatograph. The concentrations of sulfonate ion and sulfate ions in blank samples of group 1 and 2 were both 0,

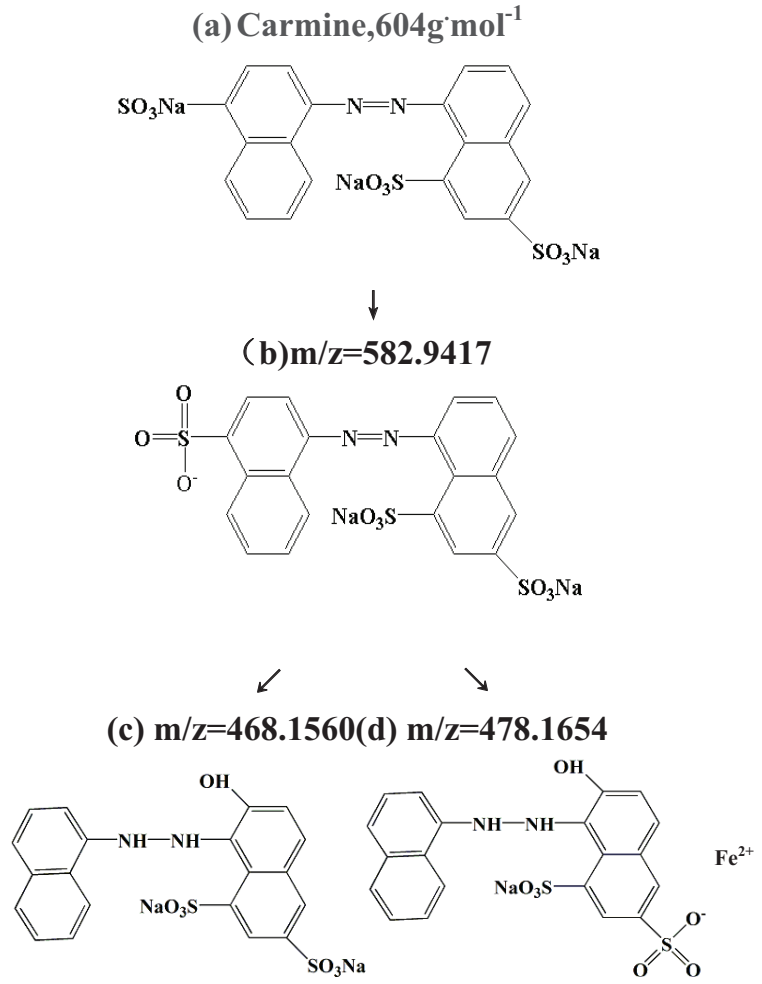


Fig. 9. Mass spectra of degraded carmine by zero-valent iron at different time. A. 0 min; B. 240 min; C. 480 min; D. 1440 min.

indicating that neither the ZVI nor the carmine solution contained sulfonate or sulfate ions. $SO_3H^-$ and $SO_4^{2-}$ were present in the third group of samples, which should be ascribed the action of the ZVI the reaction process.

Fig. 10 depicts a possible process of the degradation of carmine molecule by ZVI. Fig. 10a shows the molecular structure of carmine, with a mass-to-charge ratio of 604 m/z; b shows anionic carmine with one sodium ion removed, and a mass-to-charge ratio of 582.9 m/z; c shows the molecule with the whole sodium sulfonate group removed, and a mass-to-charge ratio of 468 m/z; d shows the anionic carmine with two sodium ions removed and an iron ion from oxidized ZVI exchanged for a sodium ion, with a mass-to-charge ratio of 478 m/z; c and d are both ZVI degradation carmine products.

Combined *IC* and *HPLC-MS* results show that the product was basically stable as two substances after 240 min, with mass-to-charge ratios of 468 m/z and 478 m/z. At a reaction time of 60 min, the color of the solution almost faded and the decolorizing efficiency reached 99%, indicating that the azo double bond was broken at 60 min. Mass spectrometry showed that the intermediate product of m/z = 478 appeared when ZVI degraded carmine for 240 min may be obtained by the exchange of $Fe^0$ oxidation into $Fe^{2+}$ and two $Na^+$ in the molecules of carmine. This is the complexation of $Fe^{2+}$ with carmine causing the $Na^+$ and sulfonate groups to fall off and $Fe^{2+}$ to occupy this position. The substance with a mass-to-charge ratio of 468 m/z is the product of the carmine dye molecule after removing a sodium sulfonate group.

ZVI is a chemically active metal with strong reduction ability, and its standard reduction potential is –0.44 V [45]. Under strong acid conditions, $Fe^0$ is easily oxidized to $Fe^{2+}$, and $Fe^{2+}$ is also reducible. The reduction reaction path mainly comprises the following steps: 1. The reactant diffuses from the solution body to the ZVI surface; 2. The ZVI adsorbs that reactant on its surface; 3. Reduction reaction of ZVI and the reactant on the iron surface; 4. Breakage of the azo double bond and conversion into small molecular organic substances [46].

The precipitation of $Fe^{2+}$ and $Fe^{3+}$ can also degrade carmine dye molecules, but the reduction, degradation, precipitation and flocculation of the carmine molecule were mainly driven by the ZVI. The chromophoric groups of dyes, such as vinyl –C=C–, azo –N=N–, hydroxyl =C=O, nitroso –N= O, etc., are strong ligands capable of complexing with ferrous ions in the transition element. The equation for decomposition of the azo dye molecule by cleavage is as follows:

$$–N=N– + 2H^+ + 2e^- \rightarrow –NH_2 + NH_2–$$

Under aerobic conditions, $O_2$ acts as an oxidizing agent to promote the corrosion of ZVI as in Eq. (11). Under oxygen-free conditions, water alone acts as an oxidizing agent to promote iron corrosion, as in Eq. (12) [46].

$$Fe^0 + \frac{1}{2}O_2 + H_2O \rightarrow Fe^{2+} + 2OH^- \quad (11)$$

$$Fe^0 + 2H_2O \rightarrow Fe^{2+} + H_2 + 2OH^- \quad (12)$$

The mechanism of purification of carmine by ZVI is as follows: 1. Reduction of ZVI. The strong reducibility of the ZVI produces new [H] and $Fe^{2+}$ by the reaction of ZVI with water under acidic conditions, and ZVI can form a micro battery with a plurality of components in the dye waste water. The azo double bond of carmine is reduced to a single bond, achieving approximately 99% decoloring; 2. Intercalation of dye anions between layered double hydroxide layers. $Fe(OH)_2$ and $Fe(OH)_3$ generated by the reaction of ZVI with water and oxygen are converted into green rust. This green rust layer has a higher structural negative charge, and the carmine anion enters into the structural interlayer to balance the structural negative charge; 3. Iron hydroxide adsorption of carmine; 4. The complexation and reduction of ferrous ions.

## 4. Conclusion

Zero-valent iron prepared by the hydrogen reduction method is of great significance for the degradation of organic dye wastewater. The results showed that ZVI exhibited an excellent degradation of color and TOC under the conditions of pH 2, solid-liquid ratio of 1 g/L, and room temperature (298K). The color removal effect reached 99% after 60 min reaction time, and the removal efficiency of TOC was approximately 57% at 1440 min. The removal of chromaticity by ZVI followed first-order reaction kinetics, and absorption kinetics and isotherms fitted well with pseudo-second order kinetics and the Freundlich models, respectively. ZVI exhibits good chemical activity for the degradation of carmine and is a good candidate for the degradation of other organic pollutants. This work provides important information for the application of ZVI prepared by modification of hematite as an environmental protection material.

## Acknowledgement

This study was financially supported by the National Natural Science Foundation of China (No. 41772038, 41572029).

## References

[1] S. Ren, J. Guo, G. Zeng, G. Sun, Decolorization of triphenylmethane, azo, and anthraquinone dyes by a newly isolated Aeromonas hydrophila strain, Appl. Microbiol. Biotechnol., 72 (2006) 1316–1321.

[2] C.A. Martínez-Huitle, E. Brillas, Decontamination of wastewaters containing synthetic organic dyes by electrochemical methods: A general review, Appl. Catal., B Environ, 87 (2009) 105–145.

[3] J. Gao, Q. Zhang, K. Su, J. Wang, Competitive biosorption of Yellow 2G and Reactive Brilliant Red K-2G onto inactive aerobic granules: Simultaneous determination of two dyes by first-order derivative spectrophotometry and isotherm studies, Bioresour. Technol., 101 (2010) 5793–5801.

[4] I. Grčić, S. Papić, K. Žižek, N. Koprivanac, Zero-valent iron (ZVI) Fenton oxidation of reactive dye wastewater under UV-C and solar irradiation, Chem. Eng. J., 195–196 (2012) 77–90.

[5] Y. Zhang, Y. Liu, Y. Jing, J. Zhao, X. Quan, Steady performance of a zero valent iron packed anaerobic reactor for azo dye wastewater treatment under variable influent quality, J. Environ. Sci., 24 (2012) 720–727.

[6] K. Balapure, N. Bhatt, D. Madamwar, Mineralization of reactive azo dyes present in simulated textile waste water using down flow microaerophilic fixed film bioreactor, Bioresour. Technol., 175 (2015) 1–7.

[7] Y. He, J.F. Gao, F.Q. Feng, C. Liu, Y.Z. Peng, The comparative study on the rapid decolorization of azo, anthraquinone and triphenylmethane dyes by zero-valent iron, Chem. Eng. J., 179 (2012) 8–18.

[8] P.A. Deshpande, S. Polisetti, G. Madras, Rapid synthesis of ultrahigh adsorption capacity zirconia by a solution combustion technique, Langmuir, 27 (2011) 3578–3587.

[9] M.M. Hossain, M.I. Mahmud, M.S. Parvez, Impact of current density, operating time and pH of textile wastewater treatment by electrocoagulation process, J. Environ. Sci., 18 (2013) 157–161.

[10] S. Meric, H. Selcuk, V. Belgiorno, Acute toxicity removal in textile finishing wastewater by Fenton's oxidation, ozone and coagulation-flocculation processes, Water Res., 39 (2005) 1147–1153.

[11] S. Suarez, J.M. Lema, Pre-treatment of hospital wastewater by coagulation-flocculation and flotation, Bioresour. Technol., 100 (2009) 2138–2146.

[12] E.S. Z. El-Ashtoukhy, N.K. Amin, O. Abdelwahab, Treatment of paper mill effluents in a batch-stirred electrochemical tank reactor, Chem. Eng. J., 146 (2009) 205–210.

[13] A. Pirkarami, M.E. Olya, N.Y. Limaee, Decolorization of azo dyes by photo electro adsorption process using polyaniline coated electrode, Prog. Org. Coat., 76 (2013) 682–688.

[14] L. Woeijye, A.F. Ismail, Polymeric nanofiltration membranes for textile dye wastewater treatment: preparation, performance evaluation, transport modelling, and fouling control - a review, Desalination, 245 (2009) 321–348.

[15] K. Yasmin, M. Kalpana, B. Shaik, J. Bhavanath, Kinetics, equilibrium and thermodynamic studies on biosorption of hexavalent chromium by dead fungal biomass of marine Aspergillus niger, Chem. Eng. J., 145 (2009) 489–495.

[16] R.A. Damodar, S.J. You, S.H. Ou, Coupling of membrane separation with photocatalytic slurry reactor for advanced dye wastewater treatment, Sep. Purif. Technol., 76 (2010) 64–71.

[17] A.K. Verma, R.R. Dash, P. Bhunia, A review on chemical coagulation/flocculation technologies for removal of colour from textile wastewaters, J. Environ. Manage., 93 (2012) 154–168.

[18] J. Cao, L. Wei, Q. Huang, L. Wang, S. Han, Reducing degradation of azo dye by zero-valent iron in aqueous solution, Chemosphere, 38 (1999) 565.

[19] S. Nam, P.G. Tratnyek, Reduction of azo dyes with zero-valent iron, Water Res., 34 (2000) 1837–1845.

[20] S. Arabi, M.R. Sohrabi, Experimental design and response surface modelling for optimization of vat dye from water by nano zero valent iron (NZVI), Acta ChimSlov., 60 (2013) 853.

[21] H. Liu, M. Li, T. Chen, C. Chen, N.S. Alharbi, T. Hayat, D. Chen, Q. Zhang, Y. Sun, New synthesis of nZVI/C composites as an efficient adsorbent for the uptake of U(VI) from aqueous solutions, Environ. Sci. Technol., 51 (2017) 9227–9234.

[22] Y. Sun, J. Li, T. Huang, X. Guan, Hematite facet confined ferrous ions as high efficient Fenton catalysts to degrade organic contaminants by lowering $H_2O_2$ decomposition energetic span, Appl. Catal. B: Environ., 100 (2016) 277–295.

[23] Y. Zhang, Y. Jing, J. Zhang, L. Sun, X. Quan, Performance of a ZVI-UASB reactor for azo dye wastewater treatment, J. Chem. Technol. Biotechnol., 86 (2011) 199–204.
[24] Y. Mamindy-Pajany, C. Hurel, N. Marmier, M. Roméo, Arsenic (V) adsorption from aqueous solution onto goethite, hematite, magnetite and zero-valent iron: Effects of pH, concentration and reversibility, Desalination, 281 (2011) 93–99.
[25] X. Huang, X. Hou, J. Zhao, L. Zhang, Hematite facet confined ferrous ions as high efficient Fenton catalysts to degrade organic contaminants by lowering $H_2O_2$ decomposition energetic span, Appl. Catal. B: Environ., 181 (2016) 127–137.
[26] H. Liu, T. Chen, Q. Xie, X. Zou, C. Chen, R.L. Frost, The functionalization of limonite to prepare NZVI and its application in decomposition of p-nitrophenol, J. Nanopart. Res., 17 (2015) 1–18.
[27] Y. Zou, X. Wang, A. Khan, P. Wang, Y. Liu, A. Alsaedi, T. Hayat, X. Wang, Environmental remediation and application of nanoscale Zero-Valent Iron and its composites for the removal of heavy metal ions: a review, Environ. Sci. Technol., 50 (2016) 7290–7304.
[28] M. Li, H. Liu, H. Zhu, H. Gao, S. Zhang, T. Chen, Kinetics and mechanism of Sr(II) adsorption by Al-$Fe_2O_3$: Evidence from XPS analysis, J. Mol. Liq., 233 (2017) 364–369.
[29] Y. Xi, Z. Sun, T. Hreid, G.A. Ayoko, R.L. Frost, Bisphenol A degradation enhanced by air bubbles via advanced oxidation using in situ generated ferrous ions from nano zero-valent iron/palygorskite composite materials, Chem. Eng. J., 247 (2014) 66–74.
[30] N. Yuan, G. Zhang, S. Guo, Z. Wan, Enhanced ultrasound-assisted degradation of methyl orange and metronidazole by rectorite-supported nanoscale zero-valent iron, Ultrason. Sonochem., 28 (2016) 62–68.
[31] L.J. Matheson, P.G. Tratnyek, Reductive dehalogenation of chlorinated methanes by iron metal, Environ. Sci. Technol., 28 (1994) 2045–2053.
[32] G.B. Ortiz de la Plata, O.M. Alfano, A.E. Cassano, 2-Chlorophenol degradation via photo Fenton reaction employing zero valent iron nanoparticles, J. Photochem. Photobiol., A: Chem., 233 (2012) 53–59.
[33] Y. Lin, C. Weng, F. Chen, Effective removal of AB24 dye by nano/micro-size zero-valent iron, Sep. Purif. Technol., 64 (2008) 26–30.
[34] Y. Liu, F. Yang, P.L. Yue, G. Chen, Catalytic dechlorination of chlorophenols in water by palladium/iron, Water Res., 35 (2001) 1887–1890.
[35] Z. Chen, T. Wang, X. Jin, Z. Chen, M. Megharaj, R. Naidu, Multifunctional kaolinite-supported nanoscale zero-valent iron used for the adsorption and degradation of crystal violet in aqueous solution, J. Colloid Interface Sci., 398 (2013) 59–66.
[36] W. Cheng, C. Ding, Y. Sun, M. Wang, The sequestration of U(VI) on functional β -cyclodextrin-attapulgite nanorods, J. Radioanal. Nucl. Chem., 302 (2014) 385–391.
[37] Y. Sun, C. Ding, W. Cheng, X. Wang, Simultaneous adsorption and reduction of U(VI) on reduced graphene oxide-supported nanoscale zerovalent iron, J. Hazard. Mater., 280 (2014) 399–408.
[38] Z. Qiang, H.B. Liu, T.H. Chen, C. Dong, M.X. Li, C. Chen, The synthesis of NZVI and its application to the removal of phosphate from aqueous solutions, Water Air Soil Pollut., 228 (2017) 321.
[39] Z. Hua, Y.B. Jiang, G.M. Zeng, Z.F. Liu, L.X. Liu, L. Yang, Y. Xin, M.Y. Lai, Y.B. He, Effect of low-concentration rhamnolipid on adsorption of Pseudomonas aeruginosa ATCC 9027 on hydrophilic and hydrophobic surfaces, J. Hazard. Mater., 285 (2015) 383–388.
[40] J. Su, S. Lin, Z. Chen, M. Megharaj, R. Naidu, Dechlorination of p-chlorophenol from aqueous solution using bentonite supported Fe/Pd nanoparticles: Synthesis, characterization and kinetics, Desalination, 280 (2011) 167–173.
[41] J. Lin, M. Sun, X. Liu, Z. Chen, Functional kaolin supported nanoscale zero-valent iron as a Fenton-like catalyst for the degradation of Direct Black G, Chemosphere, 184 (2017) 664–672.
[42] M. Aliabadi, K. Morshedzadeh, H. Soheyli, Removal of hexavalent chromium from aqueous solution by lignocellulosic solid wastes, Int. Environ. Sci. Technol., 3 (2006) 321–325.
[43] A.K. Bhattacharya, T.K. Naiya, S.N. Mandal, S.K. Das, Adsorption, kinetics and equilibrium studies on removal of Cr(VI) from aqueous solutions using different low-cost adsorbents, Chem. Eng. J., 137 (2008) 529–541.
[44] J. Lin, M. Sun, X. Liu, Z. Chen, Functional kaolin supported nanoscale zero-valent iron as a Fenton-like catalyst for the degradation of Direct Black G, Chemosphere, 184 (2017) 664.
[45] S.G. Bratsch, Standard Electrode potentials and temperature coefficients in water at 298.15 K, J. Phys. Chem. Ref. Data, 18 (1989) 1–21.
[46] J. Dong, Y.S. Zhao, R. Zhao, R. Zhou, Effects of pH and particle size on kinetics of nitrobenzene reduction by zero-valent iron, J. Environ. Sci., 22 (2010) 1741–1747.